Available online at www.sciencedirect.com

ScienceDirect

Ceramics International 40 (2014) 1001–1012

CERAMICS INTERNATIONAL

www.elsevier.com/locate/ceramint

The influence of new wet synthesis route on the morphology, crystallinity and thermal stability of multiple ions doped nanoapatite

K. Jamuna-Thevi[a,b], N.M. Daud[b], M.R. Abdul Kadir[b], H. Hermawan[b,*]

[a]Advanced Materials Research Center (AMREC), SIRIM Berhad, Kulim, Kedah, Hi-Tech Park, 09000 Kulim, Malaysia

[b]Medical Implant Technology Group (MediTeg), Faculty of Biosciences and Medical Engineering, Universiti Teknologi Malaysia, 81310 Johor Bahru, Johor, Malaysia

Received 5 May 2013; received in revised form 13 May 2013; accepted 26 June 2013
Available online 2 July 2013

Abstract

The synthesis of multiple ions doped nanoapatite powder was carried out by wet precipitation technique. A newly developed reaction route with self-controlled pH at high reaction temperatures, i.e. 37 & 85 ± 2 °C was compared to the conventional synthesis route at 37 ± 2 °C. The XRD peaks were very broad, indicating the presence of nanocrystalline apatite. The primary particle size of the powder was in the range of 20–30 nm whereas the fraction of crystallinity was between 0.20 and 0.63. TEM and SEM characterizations confirmed the nanosized primary particles of the apatite samples. The high temperature synthesis at 37 & 85 ± 2 °C improved both crystallite size and crystallinity of the as-prepared samples. A highly crystalline HA phase was formed in the ions doped samples without secondary phases, indicating its thermal stability at 900 °C in both CO_2 and air atmosphere. The in vitro cytocompatibility of the synthesised nanoapatite powders was confirmed by cell viability of human skin fibroblasts.

Keywords: Ionic doped nanoapatite; Wet precipitation; Concentration; Temperature; Fibroblast

1. Introduction

It is well known that biological apatites in a human bone are non-stoichiometric ion substituted calcium-deficient apatites [1]. It is embedded with alkali ions such as Na^+ (0.5–1 wt%), Mg^{2+} (0.4–1.2 wt%), K^+ (0.03–0.08 wt%), and CO_3^{2-} (3–8 wt%) at trace levels, where the amount of ionic substitution in the biological apatite of a human may vary individually [2–4]. Although the substitution is at trace level, these ions play an important role in biological responses of bone cells [2]. Therefore, these studies regarding substitution of these elements have become the subject of interest, lately [3].

Hydroxyapatite (HA) is a well known biomedical material for bone implantation and bone regeneration due to its excellent biocompatibility [4,5]. Several studies regarding the employment of a co-substituted HA with ionic pairs comprising of Mg^{2+}/CO_3^{2-} and Na^+/CO_3^{2-} have been reported, concentrating on one type of cation and anion substitution in HA [6]. Multiple ions (i.e. Mg, Na, Si and K) substituted calcium phosphates were also reported, but lacking the details of simultaneous substitution of CO_3^{2-} in the presence of all cations in the conventional wet precipitation technique [6–8]. The major concern in simultaneous multiple ion substitutions is the competition that arises between atoms to occupy the crystal structure [9]. The fraction of Na^+ is not quantitatively revealed although largely introduced in the initial synthesis of Sr, Mg and CO_3^{2-} substituted hydroxyapatites [6,10]. A literature report on potassium substituted hydroxyapatite showed no significant changes in the phase behaviour of resultant apatites. However, this study was not focused on the effects of co-substitution of CO_3^{2-} [3]. Many techniques for synthesising HA were described in earlier works such as sol–gel, wet precipitation and solid-state reaction techniques [11–14]. Sol–gel synthesis often leads to thermal instability of the HA phase despite its homogenous composition [15]. In a solid-state reaction, the long duration and comparatively high annealing temperatures were the main drawbacks [14]. The wet precipitation technique was advantageous due to its more

*Corresponding author at: Tel.: +60 7 5558493; fax: +60 7 5558515.
E-mail address: hendra.hermawan@biomedical.utm.my (K. Jamuna-Thevi).

0272-8842/$ - see front matter © 2013 Elsevier Ltd and Techna Group S.r.l. All rights reserved.
http://dx.doi.org/10.1016/j.ceramint.2013.06.097

convenient preparation procedures, resulting in a pure homogenous HA with comparatively good crystallinity [4,16].

The substituents in the apatite structure influence the particle morphology, powder crystallinity, stoichiometry and thermal stability of the precipitates [2,9,17]. Silicate and Mg were found to reduce HA crystallinity and inhibit HA nucleation and growth [18]. High sinterability and decomposition temperature were dependent on powder characteristics of the HA that are correlated strongly with the sintering density and mechanical properties [4]. Therefore, it is highly essential to obtain a material with controlled powder morphology, crystallinity and chemical composition for the application of substituted HA as a bioceramic material. In the wet precipitation method, major parameters concerned were reactant concentration, reaction temperature, addition rate, stirring and maturation that tailored to meet the raw HA preparation [19]. The synthesis of HA particles with desired properties such as thermal stability and mechanical property by varying the reactant concentration, pH and reaction temperature has been reported. However, the HA was precipitated at high pH (>12) control using ammonia [4]. The HA precipitation at "self-controlled" high pH without the utilisation of alkali agents makes the whole synthesis easier and more suitable for industrialisation, using classical neutralization route involving calcium hydroxide and orthophosphoric acid [6,10]. However, the latter was a low crystalline HA synthesised at low temperature (<40 °C) to self-stabilize high pH. Infact, there were no report on the systematic study focusing on the effects of chemical reaction at high temperature and various reactant concentrations on simultaneous doping of Na, Ma, K and CO_3^{2-} in nanoapatites, using a wet precipitation of $Ca(OH)_2$ and phosphoric acid with self-stabilizing pH without addition of ammonia.

Application of as-prepared low crystalline HA nanoparticles in biomedical field require the final form to be neutral, but without any presence of other chemical such as ammonia. In this study, a new and simple wet precipitation technique with "self-controlled" pH but without addition of ammonia was employed to prepare multiple ions doped nanoapatite by varying the reactant concentration at high temperature during the synthesis. The effects of synthesis temperature and reactant concentration on the formation, morphology, crystallinity and thermal stability of multiple ions doped nanoapatite were examined. A cytotoxicity test with extract of the materials was performed to evaluate the presence and/or release of toxic leachables and degradation products.

2. Materials and methods

2.1. Material synthesis

The synthesis route for both stoichiometric nanohydroxyapatite (as control) and non-stoichiometric ion doped nanoapatite were modified based on other works [6,7]. Calcium hydroxide ($Ca(OH)_2$; Fluka, USA, purity $>96\%$), orthophosphoric acid (H_3PO_4; Merck, USA, purity minimum 85%), sodium hydrogen carbonate ($NaHCO_3$; Merck, USA, purity=99.5%), magnesium chloride hexahydrate ($MgCl_2 \cdot 6H_2O$; Merck, USA, purity=98%) and potassium chloride (KCl; Merck, USA, purity=99.5%) were used as starting precursors for the synthesis. Two different types of compositions (NApF1 and NApF2) were used to attempt the ions doped nanoapatite synthesis (Table 1), where the equimolar concentration of Ca and P was varied at 1.0, 1.5 and 2.0 M, while other additives remained constant. The synthesis was carried out using two different reaction methods with self-stabilised pH control which involved: (I) a continuous reaction at 37 ± 2 °C with pH 7–12 and maintained constant for 2 h, and a new method; (II) initial reaction at 37 ± 2 °C until completion of ions addition, followed by an increase in reaction temperature at 85 ± 2 °C with pH 6–12 and maintained constant for 2 h, i.e. denoted as 37 and 85 °C ± 2 °C. An appropriate amount of a PO_4^{3-} ionic solution was added slowly together with a Na^+ and a CO_3^{2-} ionic solution (1–2 drops/s) into the basic suspension containing Ca^{2+}, Mg^{2+} and K^+ precursors, stirred at 400 rpm and heated using either reaction methods I or II. The suspension was maintained under stirring at a constant temperature for 2 h, then left to cool to room temperature for 24 h without stirring to age the precipitated product. The precipitation product was filtered and washed for 3 times using 1.5 L of double distilled de-ionised water at each wash until the filtrate pH was almost 7–8. The filtered cake was then dried at 80 °C for 24 h. The dried cake was crushed, ground to fine powders and sieved through 500 μm mesh size. Similarly, synthesis of stoichiometric nanohydroxyapatite (NHA) was carried out by adding appropriate amounts of Ca^{2+} and PO_4^{3-}, where the Ca/P ratio was fixed at 1.67. The powder samples

Table 1
Molar concentration of precursors used in the synthesis.

Formulation 1 (NApF1)			Formulation 2 (NApF2)		
Elements	Mole	wt%	Elements	Mole	wt%
Ca	1.0	40.08	Ca	1.0	40.08
P	0.6	18.58	P	0.6	18.58
Na	0.04	0.90	Na	0.08	1.84
Mg	0.03	0.72	Mg	0.06	1.46
K	0.000767	0.03	K	0.001534	0.06
CO_3^{2-}	0.04	2.40	CO_3^{2-}	0.08	4.80
Ca/P molar ratio	1.67	–	Ca/P molar ratio	1.67	–
(Ca+Na+Mg+K)/P ratio	1.78	–	(Ca+Na+Mg+K)/P ratio	1.90	–

were heat treated between 900 and 1250 °C, at a ramp rate of 5 °C/min for 1 h in air and CO_2 controlled atmospheric condition. Then, the samples were subjected to physico-chemical characterisations.

2.2. Powder characterisation

Phases of the apatite powders were determined and recorded by an X-ray Diffractometer (XRD; Bruker D8 Advance, Germany) at ambient temperature using Ni-filtered Cu-Kα radiation ($\lambda = 0.15406$ nm). Data were collected in the range of 25°–55° (2θ), with a step of 0.02° and a scanning rate of 1.2° per minute. The samples were ground finely into a powder form using an agate mortar and spread over the analytical cylindrical sample holder. The powder surface was smeared uniformly on the sample holder to obtain a flat upper surface. Then, the spread surface was characterised by analysing the characteristic peaks of the phases present. The size of individual apatite crystallites were calculated from XRD data using the Scherrer Eq. (1). The peak assigning to (002) Miller's plane family was chosen for calculation of crystallite size since it is sharper and isolated from others. It is also shows the crystal growth along the *c*-axis of the apatite crystalline structure

$$X_s = \frac{K\lambda}{(\mathrm{FWHM}_{002}) \times \cos\,\theta} \quad (1)$$

where X_s is the crystallite size as calculated for the (hkl) reflection. λ is the wavelength of the monochromatic X-ray beam (nm) ($\lambda = 1{:}5406$ Å for Cu Kα radiation), FWHM is the full width at half maximum for the diffraction peak under consideration (rad) and θ the diffraction angle (°) and k is the broadening constant varying with crystal habit and chosen as 0.9 for the elongated apatite crystallites. The crystallinity noted by X_c corresponds to the fraction of crystalline apatite phase in the investigated volume of the powdered sample. An empirical relation between X_c and the FWHM was deduced, according to

$$\mathrm{FWHM}_{(002)} \times \sqrt[3]{X_c} = K \quad (2)$$

where X_c is the crystallinity degree, FWHM is the full width of the peak at half intensity of (002) reflection in (2θ°), K is a constant found equal to 0.24 for a very large number of different HA powders.

The changes in the crystal structure (lattice parameters) were quantified based on interplanar distances (d values) obtained by XRD (peak 25–27° = 002 plane; peak 28–30° = 210 plane; peak 32–34° = 300 plane; peak 39–41° = 310 plane; peak 52–54° = 004 plane). This allowed the calculation of the parameters a and c from the crystal lattice following:

$$\lambda = 2d_{hkl} \sin\theta_{hkl} \quad (3)$$

$$\frac{1}{d_{hkl}^2} = \frac{4}{3}\left(\frac{h^2 + hk + 1^2}{a^2}\right) + \frac{1^2}{c^2} \quad (4)$$

IR spectra of the powders were obtained by attenuated total reflectance (ATR) technique using IR Fourier Spectrometry (FTIR; Perkin Elmer, Spectrum 2000, USA). A 3 mg of powder sample was placed onto the ATR sample holder and pressed down to ensure contact. All spectra were collected between 400 and 4000 cm^{-1} wavenumber region with 4 cm^{-1} resolution and 16 scans. The presence of calcium, phosphorus and ion dopants in the apatite powders were determined by inductively coupled plasma-optical emission spectrometry (ICP-AES; Perkin Elmer, Optima 7300DV, USA). The carbonate contents of the as-prepared and heat-treated powders were measured by CHN analysis using a CHN elemental analyzer (CHN analyzer; Elementar, Vario EL III, Germany). The morphology of apatite powder particles were examined using a Field-Emission Scanning Electron Microscope (FESEM; Leo 1525, Germany). Prior to this examination, the powders were coated with platinum using a sputter coater to prevent charging on particle surfaces in the SEM. The particle size and morphology of as-prepared powders were analysed using a Transmission Electron Microscope (TEM; Philips Tecnai 20S-Twin, Netherlands). The powder samples were dispersed by ultrasonicating apatite particles in isopropanol for 10 min before placing one drop of the sample on a carbon coated copper grid. Thermal behaviour of the powders was studied by thermal gravimetric analysis and differential thermal analysis (TGA/DTA; Exstar 6000, Japan) between 25 and 1200 °C in air at a heating rate of 5 °C/min. The specific surface area of the powders was measured by the Brunauner–Emmett–Teller (BET) gas adsorption method (Quantachrome Instruments; Autosorb-1C, USA). Sample outgassing was performed at 110 °C for 24 h prior to analysis. The particle size distribution of the powders was analysed by a dry laser particle size analyser (Cilas 1190, France), using dry jet dispersion operating pressure of 1000 mbar for 15 s to deagglomerate the powder particles.

2.3. Cytotoxicity testing

Human Skin Fibroblast cells (HSF 1184) were purchased (European Collection of Cell Cultures (ECACC), UK) and cultured at passage six with Minimum Essential Medium (MEM) (Gibco, Life Technologies, USA) containing 10% fetal bovine serum and 1% penicillin/streptomycin at 37 °C in a 5% (v/v) CO_2 incubator. The medium was changed every 3 days until confluence. After 80% of confluency, they were subcultured by detaching cells with 0.25% (w/v) Trypsin-EDTA (Sigma Aldrich, USA). Cytotoxicity tests were carried out using a test extract on a confluent monolayer culture of cells, also known as indirect contact method. The preparation of a sample extract is based on the guidelines in ISO 10993-12 (Biological evaluation of medical devices-Part 12). The NHA-1.5M and NApF2-1.5M powder samples, which were synthesised at 37 and 85 °C ± 2 °C (reaction method II), extracted in completed culture medium (MEM supplemented with 10% fetal bovine serum and 1% penicillin/streptomycin) for 24 h at 37 °C. The lower concentrations of a sample solution (100 μg) were diluted from a sample solution with higher concentration (300 μg). These extracts were then used immediately for cytotoxic tests. The cell suspension was adjusted to a density of 3×10^4 cell/ml; in addition, 1 ml of cell suspension together

with 1 ml of extract of each concentration was added into 12-well plates. After cells were incubated in humidified atmosphere with 5% CO_2 at 37 °C for 24 h, 100 µl of 5 mg/ml 3-(4,5-Dimethylthiazol-2-yl)-2,5-diphenyltetrazolium bromide (MTT) solution (Invitrogen, USA) was added to each well, and the plates were placed into an incubator for 4 h. A dimethyl sulfoxide (DMSO) (Biobasic, Canada) solution (1 ml) was added into plates after removing the MTT solution. The MTT, a yellow tetrazolium salt, was enzymatically converted by a living cell to a purple formazan product, where its colour intensity is directly proportional to the number of viable and proliferation of cells in vitro. The spectrophotometrical absorbance of the specimens was measured with a microplate reader (BioTek ELx808, USA) at 570 nm.

3. Results and discussion

3.1. Phase evaluation, elemental analysis and morphology of as-prepared powders

The broad diffraction peaks were observed for a poorly crystalline ions doped apatite powder (NApF2-1.5M) synthesised at 37 ± 2 °C (reaction method I), which also suggested that the apatite particles are nanosized (Fig. 1). As the synthesis temperature increased and then maintained at 85 ± 2 °C (reaction method II), these diffraction peaks become more intense, indicating an increase in crystallinity and crystallite size of the apatite powders as evidenced in Table 2. The crystal size in the wide dimension along the *c*-axis of HA crystallites and their corresponding crystallinity degree were evaluated using the line broadening of the (002) reflection because this peak is well resolved and shows no interferences [20]. The synthesis of ions doped apatite by fixing the Ca/P molar ratio at 1.67 and mixing the equimolar (1.5 M) of Ca and P precursors at both reaction temperatures have exhibited the presence of pure HA without any traces of secondary phases in the "as-prepared" samples.

In order to study the effect of molar concentration, equimolar (1.0, 1.5 and 2.0 M) Ca and P precursors with fixed Ca/P molar ratio = 1.67 were used to synthesise the ionic doped apatite (NApF2) at 37 & 85 ± 2 °C. Fig. 2 shows the XRD pattern of as-prepared powders that consist of pure HA without secondary phases. As the precursor concentration

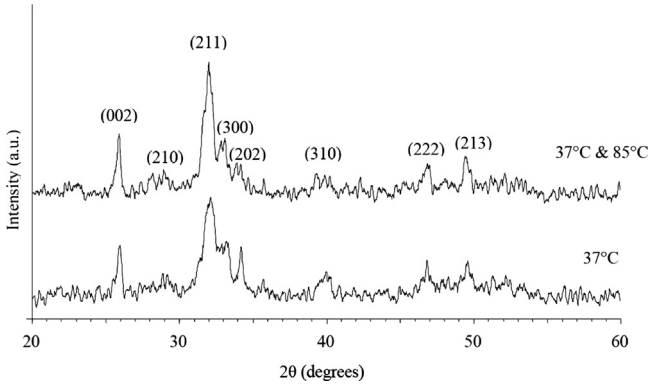

Fig. 1. XRD patterns of as prepared ionic doped apatite (NApF2) synthesised at 37 ± 2 °C (reaction method I) and 37 and 85 ± 2 °C (reaction method II).

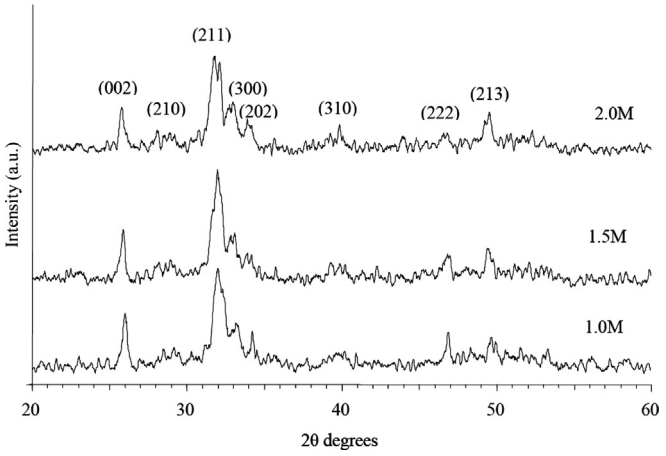

Fig. 2. XRD patterns of as prepared ionic doped apatite (NApF2) synthesised at 37 & 85 ± 2 °C (reaction method II) using 1.0M, 1.5 M and 2.0 M equimolar precursors.

Table 2
Effect of various synthesis parameters on crystallite size, crystallinity, specific surface area and lattice parameters of as prepared stoichiometric HA (NHA) and ionic doped apatite (NApF1 and NApF2) powders.

Reaction temperature (°C)	Sample (concentration)	Crystallite size (nm)	Crystallinity (%)	Specific surface area (m^2/g)	Lattice parameters		
					a (Å)	*c* (Å)	*c*/*a*
37	NApF2 (1.5 M)	21.62	25.8	78.41	9.444	6.921	0.733
	NHA (1.0 M)	26.72	48.72	48.74	9.418	6.874	0.73
	NHA (1.5 M)	29.11	62.97	55.34	9.423	6.908	0.733
	NHA (2.0 M)	28.39	58.48	54.02	9.457	6.928	0.733
	NApF1 (1.0 M)	20.12	20.81	84.93	9.422	6.901	0.732
37 and 85	NApF1 (1.5 M)	25.8	43.81	77.37	9.41	6.893	0.733
	NApF1 (2.0 M)	25.31	41.41	78.95	9.41	6.907	0.734
	NApF2 (1.0 M)	23.16	31.7	82.09	9.373	6.862	0.732
	NApF2 (1.5 M)	25.32	41.41	85.72	9.418	6.892	0.732
	NApF2 (2.0 M)	23.97	35.17	84.47	9.421	6.951	0.738

increased from 1.0 to 2.0 M, the diffraction peaks of the as-prepared powders showed no significant changes in the powder pattern. In overall, the crystallite size of all as-prepared apatite powders were in the range of 20–30 nm whereas the crystallinity is 20–63% (Table 2). In the NApF2, both crystallite size and crystallinity increased with increasing synthesis temperature. This indicated a strong synthetic temperature dependence of the apatite precipitates. Similarly, the molar concentration also showed a slight influence on the crystallite size and crystallinity whereby both were increased by increasing the molar concentration from 1.0 to 1.5 M. However, a slight drop in both crystallite size and crystallinity was observed when the molar concentration increased to 2.0 M despite the changes in the XRD patterns (Fig. 2) that were not significantly revealed. The influence of precursor's concentration on the precipitation of HA through nucleation–aggregation–agglomeration growth process has been reported [4]. The increase in reactant concentration forms large agglomerates due to the surface minimisation of small precipitates with large surface areas. This indicates the formation of small precipitates when the molar concentration is increased, which is also in agreement with the current study that shows a decrease in the crystallite size of the apatite precipitates when the reactant concentration was increased from 1.5 to 2.0 M.

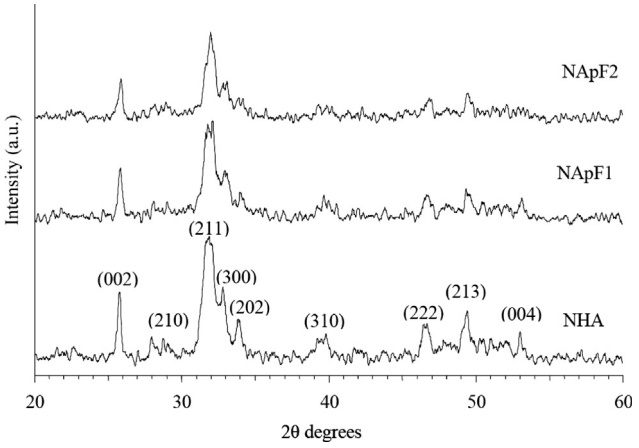

Fig. 3. XRD patterns of as prepared stoichiometric HA (NHA) and ionic doped apatite (NApF1 and NApF2) powders synthesised at 37 and 85 ± 2 °C (reaction method II) using 1.5 M equimolar precursors.

Fig. 3 shows the effect of ion dopants on the crystallinity of HA. The increasing amounts of ion dopants from 1–2 folds as in NApF1 and NApF2, (Table 1), have significantly reduced the peak intensities and broadened the XRD peaks of the substituted nanoapatite. The increasing amount of ion dopants in the HA structure slightly reduces the crystallinity of the powder particles with respect to the stoichiometric HA (NHA) as evidenced in Fig. 3. However, the temperature raise during synthesis has slightly increased the crystallinity level and crystallite size (Table 2) of the ions doped nanoapatite powders in which they provide better XRD peaks interpretation compared to powders synthesised at lower temperature.

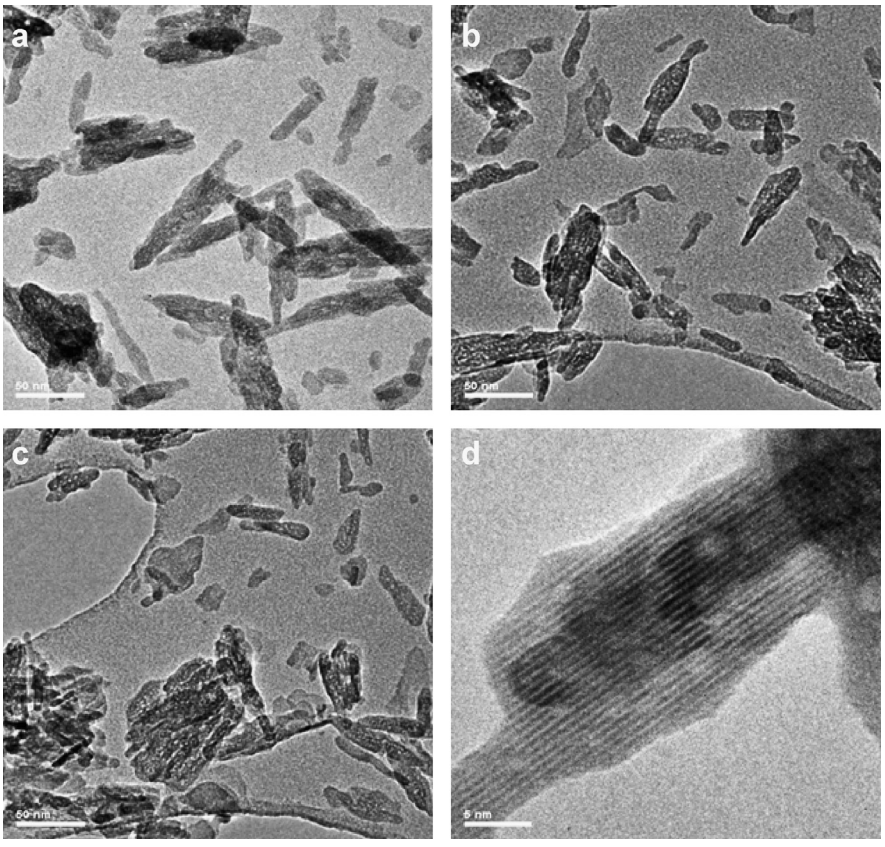

Fig. 4. TEM micrograph of as prepared HA synthesised at 37 ± 2 °C using reactant concentration (a) 1.0 M, (b) 1.5 M and (c–d) 2.0 M at low magnification (a,b,c) and high magnification (d), respectively.

This is beneficial as the ions doped nanoapatite prepared at low temperature synthesis could only achieve almost 26% crystallinity compared to almost 2 fold increase in crystallinity at high temperature synthesis (Table 2). Previously, it has been reported that the synergic effect of Mg and CO_3^{2-} dopants and low temperature synthesis had reduced the size of apatite nuclei, and inhibited crystallisation in the reaction site of the ions doped apatites compared to the stoichiometric HA [6,17]. Therefore, this study clearly evidenced that increasing the synthesis temperature and varying reactant concentration yield larger apatite nuclei with higher crystallinity compared to low temperature synthesis.

In order to confirm XRD results concerning the primary particle size of HA, TEM measurements were performed. The nanoparticle morphology of the as-prepared NHA powders synthesised using 1.0, 1.5 and 2.0 M reactant concentrations at 37 ± 2 °C showed nano-crystallites in the form of needle-like crystals as shown in TEM micrographs (Fig. 4a–d). These HA particles were absolute nanocrystals with well-defined lattice fringes. These micrographs denotes the existence of agglomeration of HA powders at nanoscale, synthesised using all reactant concentrations.

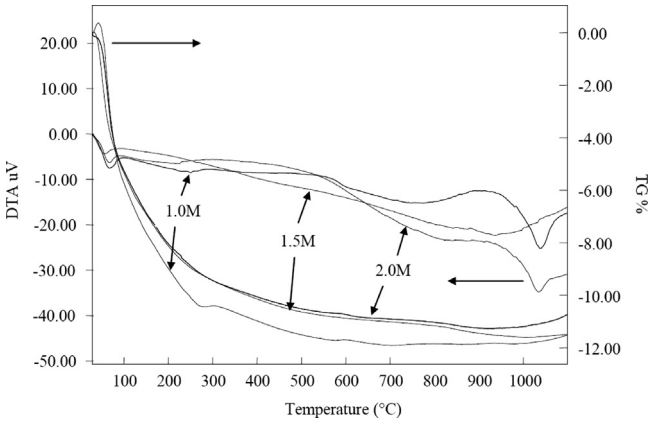

Fig. 5. TGA and DTA curves of the stoichiometric HA powders synthesised at 37 ± 2 °C using 1.0M, 1.5 M and 2.0 M reactants and dried at 80 °C.

The lattice parameters a and c (Table 2) for as-prepared apatite samples were nearly similar to the standard HA values of $a=9.418$, $c=6.884$ and $c/a=0.731$ (ICDD:9-432) and correspond to the hexagonal crystal structure. It was noted that a structural change in lattice occurred for both temperature and concentration variation were likely caused by accommodation of ionic species such as H_3O^+ due to low temperature wet chemical processes [21]. A slight decrease of cell parameters were evidenced in the as-prepared samples due to the ions substitution in the HA lattice. In particular, the as-prepared NApF2-E (85 °C) (1.5 M) showed a decrease in both a and c values with respect to as-prepared NHA-E (85 °C) (1.5 M) due to multiple ionic substitution. The c/a ratio showed a decrease from 0.733 to 0.732 due to changes in the lattice parameters of NHA and NApF2 samples respectively, indicating the ions have structurally incorporated in the HA but not just cover the surface of the crystal. This is further confirmed by the TGA-DTA analysis, which pointed out that a total mass loss was caused by water adsorption, presence of CO_3^{2-} and dehydroxylation processes during the thermal decomposition. Various reactant concentrations showed no significant changes in the mass loss due to its thermal decomposition. TGA and DTA curves of the stoichiometric HA samples synthesised at 37 °C, using 1.0, 1.5 and 2.0 M reactant concentrations, and dried at 80 °C are shown in Fig. 5. The total mass loss in the heat-treatment process is about 11.52%, 12.56% and 11.18% in 1.0, 1.5 and 2.0 M samples, respectively, depending on the crystallinity of these samples. A relatively pronounced mass loss occurred between 25 and 200 °C is around 8.13%, 9.33% and 7.93% in 1.0, 1.5 and 2.0 M samples, respectively, with the associated broad endothermic peak that was attributed to adsorbed water [19,22]. The removal of interstitial water may also take place around 200 to 600 °C [19]. The mass loss in this range was measured around 2.75%, 2.76% and 2.70% with increasing reactant concentration. These results indicated that the amount of water adsorbed on the surface of particles was not influenced by the reactant concentration introduced during the synthesis. The decomposition of carbonate into CO_2 gas occurred from 600 to 800 °C [23], with almost constant

Table 3
Planned molar concentrations of the precursors used in the synthesis of nanoapatite compared to actual molar concentrations obtained in the as-prepared powders by varying the (Ca and P) equimolar reactant concentrations and synthesis temperature.

Elements	Planned molar concentrations (wt%)	Actual molar concentrations (wt%)			
		Synthesised at 37 and 85 ± 2 °C			Synthesised at 37 ± 2 °C
		NApF2 (1.0 M)	NApF2 (1.5 M)–R2	NApF2 (2.0 M)	NApF2 (1.5 M)
Ca	40.08	37.6	37.4	37.8	38.7
P	18.58	16.5	16.5	16.5	16.2
Mg	1.46	1.27	1.27	1.21	1.09
Na	1.84	0.16	0.16	0.18	0.15
K	0.06	0.0089	0.0103	0.0072	0.008
CO_3^{2-}	4.80	4.94	4.94	5.11	5.18
Ca/P molar ratio	1.67	1.76	1.75	1.77	1.85
(Ca+Mg+Na+K)/P molar ratio	1.90	1.87	1.86	1.88	1.94

carbonate loss at 0.29%, 0.15% and 0.30%, regardless of the reactant concentration used in the synthesis system. With increasing temperature from 800 °C to 1100 °C, the weight loss around 0.35%, 0.32% and 0.25% in 1.0, 1.5 and 2.0M samples, respectively, was negligible as shown in TGA results. This is due to the dehydroxylation process, which occurs gradually in a wide range of temperature (850–1400 °C) and can slightly contribute to the total weight loss detected by the TGA [24]. This was also confirmed by the intense endothermic peak for the DTA curve around 1000 °C. A comparison between stoichiometric HA samples synthesised using 1.5M reactant concentrations at 37 °C and 37 and 85 °C (data not shown) indicated a slight difference in total mass loss around 12.56% and 9.62%, respectively, attributed to increased water loss (adsorbed) in the former synthesis method. Therefore, it can be deduced that the increase of the synthesis reaction temperature is likely to reduce the water absorption in HA samples.

The ICP-AES and CHN elemental analysis presented in Table 3 confirmed the presence of all intended elements in the powder. All the as-prepared powders showed slight variation in the substitution of ions with prominent concentration observed for Mg, although the reactant concentrations and synthesis temperatures were varied during synthesis of NApF2 samples. The substitution of Mg is about 83% of the total amount introduced in the starting suspensions which is almost 3 folds higher than reported by others who used similar synthesis routes [6]. However, the Na and K substitutions are lower than the total amounts introduced in starting solutions. Almost similar amounts of Na and K ions were present in both NApF1 (Table 4) and NApF2 samples even though the contents of starting solutions were reduced half in NApF1, compared to NApF2 samples with Na and K ions doping between 0.58–0.75 mol% and 0.016–0.028 mol%, respectively, with respect to Ca. Although the ions doping at Ca sites showed an increase for both elements when starting solution contents were increased, the uptake of these elements decreased from 14.4 to 8.7% and 19.7 to 17.2% for Na and K ions, respectively. This indicates a reduction in ion substitutions relative to the total introduced in starting solutions. This is likely the maximum amounts of these ions entering into the nanoapatite structure in the presence of Mg and CO_3^{2-} ions, particularly using this synthesis route despite increasing the concentration of starting solution. More than 83% of Mg ions from 0.72–1.46 wt% starting solution substitute the Ca sites with Mg doping between 3.2 and 5.6 mol% with respect to Ca, where the values are close to biological apatite. This denotes that the role of Mg is more dominant in substituting Ca sites compared to Na and K ions. Mg ions are bivalent as Ca ions; therefore, carbonate is not necessarily substituted in the phosphate site to preserve the charge balance which contrarily occurs in Na and CO_3^{2-} substituted HA. The substitution of bivalent Ca^{2+} with monovalent Na^{+} stimulates the substitution of trivalent anion PO_4^{3-} with the bivalent anion CO_3^{2-} [6]. Thus, it seems that Mg is dominating the substitution level into Ca sites even though the initial content of Na starting solution is higher than Mg, i.e. Na is more concentrated than Mg. Although the Na and K contents are not up to the composition of the biological apatite, the presence of these ions at lower concentration is expected to play a role in the biochemistry of hard tissue as the ionic substitutions in the apatite phase may vary depending on the individual.

Table 4
Planned molar concentrations of the precursors used in the synthesis of nanoapatite compared to actual molar concentrations obtained in the as-prepared powders by reducing the dopants concentration (less than Table 3) and using 1.5 M (Ca and P) reactant concentrations.

Elements	Planned molar concentrations (wt%)	Actual molar concentrations (wt%) Synthesised at 37 and 85 ± 2 °C NApF1
Ca	40.08	38.8
P	18.58	16.5
Mg	0.72	0.75
Na	0.90	0.13
K	0.03	0.0059
CO_3^{2-}	2.4	3.45
Ca/P molar ratio	1.67	1.82
(Ca+Mg+Na+K)/P molar ratio	1.78	1.89

The as-prepared stoichiometric HA showed the Ca/P molar ratio of 1.68 which is in good consistency with the planned values. A slight increase in the Ca/P molar ratio of NApF1 and NApF2 samples deviating from stoichiometric HA is due to CO_3^{2-} substitution at PO_4^{3-} site, where the content was determined using the CHN analysis (Tables 3 and 4). It is obvious that the CO_3^{2-} substitution is not influenced by the reactant concentration used during synthesis as similar content of carbonate was observed at each concentration of reaction. However, the carbonate content was decreased about 23.3%, 9.21% and 4.63% for as-prepared NHA (1.69 wt%), NApF1 (3.45 wt%) and NApF2 (4.94 wt%) respectively, when the synthesis temperature was increased according to reaction method II. The carbonate drop in stoichiometric HA (NHA) is far higher than other samples since it is only dependent on unintentional addition of carbonate source from atmosphere that is largely reduced due to the lower solubility of CO_2 at high temperature [24]. An effective increase in carbonate composition was observed with the increasing carbonate source addition during the synthesis which is parallel to that of the biological hydroxyapatite (4–8 wt%).

Fig. 6 shows the FTIR spectra of the as-prepared samples corresponding to HA characteristic bands for both stoichiometric and ions doped nanoapatite. Peaks for the substitution of CO_3^{2-} at 1420 and 875 cm^{-1} for PO_4^{3-} ions were observed in all samples with more absorption intensities for samples with increasing amount of carbonate ion introduced during the synthesis [21]. Even though the CO_3^{2-} source was unintentionally introduced in NHA samples, atmospheric CO_2 reaction with high pH solution is likely the cause of CO_3^{2-} inclusion in HA [6,25]. The OH^{-} shoulder peak at 631 cm^{-1}, which is the characteristic band for HA, was only observed in stoichiometric HA samples and disappeared in ionic

substituted nanoapatites due to its low crystallinity as supported by XRD patterns (Fig. 3). It is also suggested that the decrease in intensity of OH^- vibration mode at 631 cm^{-1} as well as broadening of PO_4^{3-} bands in as-prepared ionic substituted apatites with respect to HA sample are due to the increase in lattice disorder caused by HPO_4^{2-}, which is typical for ionic substituted HA synthesised by wet precipitation methods. However, it is generally difficult to distinguish between HPO_4^{2-} and CO_3^{2-} due to the overlapping of the characteristic peak around 870 cm^{-1} [17]. A broad band around 2800–3600 cm^{-1} is due to adsorbed water whereas the stretching mode of the structural hydroxyl group, OH^- at 3570 cm^{-1} that is not visible in the spectra, might be overlapped by the broad adsorbed water bands. Bands at 1090 (shoulder peak), 1023, 963, 602 and 561 cm^{-1} are assigned to vibrations of the phosphate group, PO_4^{3-}. A band at 1647 cm^{-1} is attributed to adsorbed water in HA [26–28], whereas peaks at 2161–1971 cm^{-1} have been interpreted as combination of bands for PO_4^{3-} [29].

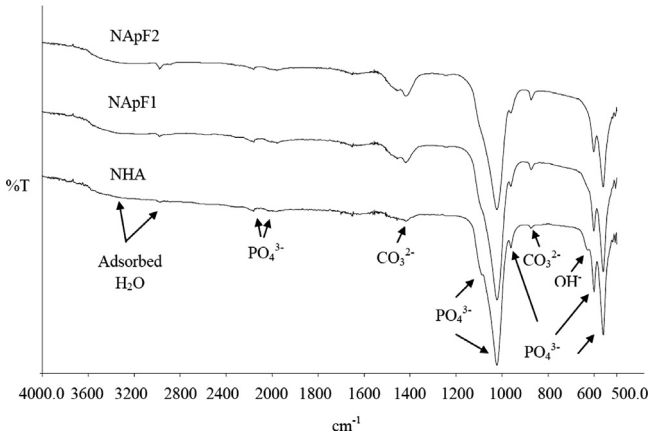

Fig. 6. FTIR of as prepared stoichiometric HA (NHA) and ionic doped apatite (NApF1 and NApF2) powders synthesised at 37 & 85 ± 2 °C (reaction method II) using 1.5 M equimolar precursors.

A comparative powder morphology of stoichiometric HA and ionic doped nanoapatite powders prepared using 1.5 M reactant concentrations at 37 & 85 ± 2 °C are illustrated in the SEM micrographs (Fig. 7). The SEM analysis of NHA, NApF1 and NApF2 powders showed that the nanoapatite powders were similarly consisting of nanometric primary particles with high tendency to agglomerate even though the dopants concentration was increased in HA. However, the morphology of these powders showed ions doped agglomerated particles formed in globular shape whereas the stoichiometric HA revealed sharper and elongated particles in agglomeration. The particle size, which also reflects the agglomerate size, seems not being affected by the synthesis temperature as the powder particles were measured between 31 and 71 μm, similar for both reaction temperatures. However, variation of the reactant concentration at 1.0 and 1.5M in 37 & 85 °C synthesis system pointed out the formation of smaller agglomerates (31–33 μm) in NApF2 samples compared to the NHA sample (65–68 μm); even though the specific surface area of ions doped apatite samples is higher than the stoichiometric HA due to smaller primary particles formation (Table 2). Smaller particles have a tendency to form large agglomerates due to the high surface area to minimise their surface energy [4,30]. Therefore, it is likely due to the easy break down of the hard agglomerates that form smaller agglomerates when jet dispersion in the particle size analyser was used to deagglomerate the powder particles in ions doped nanoapatite powders. In NHA powders, increasing the reactant concentration to 2.0 M showed a tendency of forming smaller agglomerates (~32 μm) compared to other reactant concentrations. The ionic doped apatite sample (NApF2) is observed to

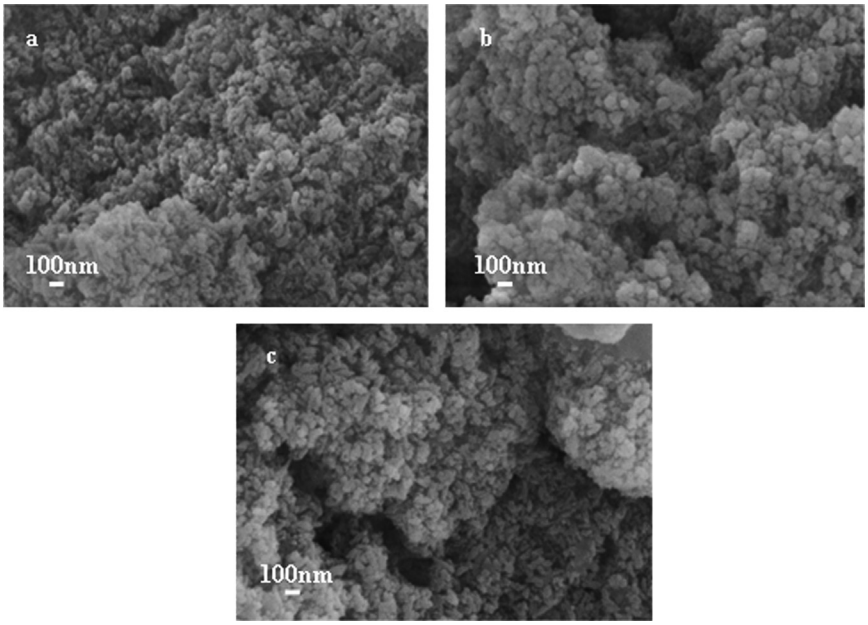

Fig. 7. SEM micrograph on the morphology of (a) stoichiometric HA (NHA), ionic doped nanoapatite (b) NApF1 and (c) NApF2 powders synthesised at 37 & 85 ± 2 °C using 1.5 M reactant concentration at 30,000 × magnification.

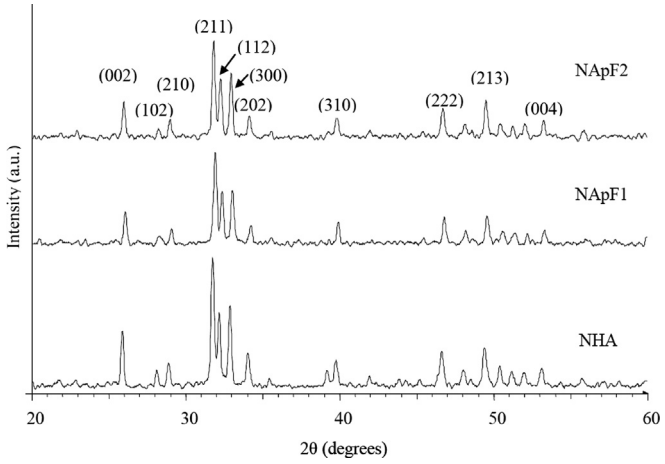

Fig. 8. XRD patterns of stoichiometric HA (NHA) and ionic doped apatite (NApF1 and NApF2) powders synthesised at 37 & 85 ± 2 °C (reaction method II) using 1.5 M equimolar precursors after heat-treatment at 900 °C in CO_2 controlled atmosphere.

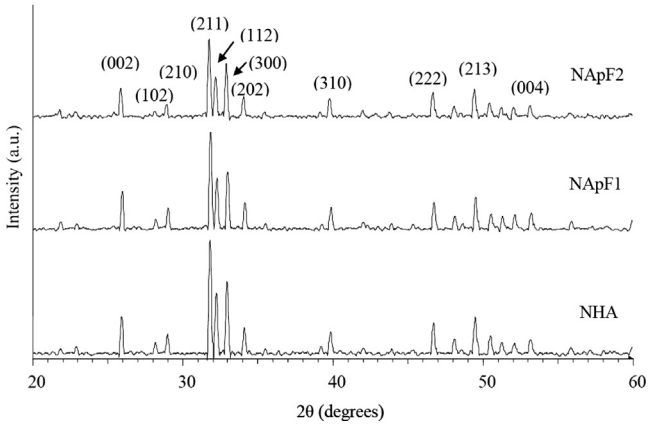

Fig. 9. XRD patterns of stoichiometric HA (NHA) and ionic doped apatite (NApF1 and NApF2) powders synthesised at 37 & 85 ± 2 °C (reaction method II) using 1.5 M equimolar precursors after sintering at 1250 °C in air.

possess smaller agglomerates (31–33 μm) at all reactant concentrations with respect to NHA sample. This denotes the tendency of easy breakdown of the apatite particles with increasing ionic dopants and reactant concentration in powder samples of NApF2 and NHA, respectively.

3.2. Thermal stability

Based on aforementioned results, preparation of NHA and NApF2 samples using 1.5 M at 37 & 85 °C showed improved crystallinity compared to other synthesis parameters. These samples were evaluated for thermal stability studies. Fig. 8 shows XRD peaks of the heat-treated ions doped apatite powders (NApF1 and NApF2) compared to the NHA at 900 °C in CO_2 controlled atmosphere. Despite the presence of ion dopants, a highly crystalline HA phase was formed without secondary phases, indicating the thermal stability of this powder without further decomposition at high temperatures, contrary to literature reports by others [7,30]. The heat-treated samples also showed significant improvement in crystallinity, with the separation of (211) and (112) diffraction peaks compared to as-prepared samples. The heat-treatment at 900 °C in CO_2 flux is to prevent carbonate loss from the material as well as to avoid decomposition of the ions doped HA phase [30]. The thermal stability of the apatite powders were further confirmed and are comparable to the stoichiometric HA as evidenced in Fig. 9 with no presence of secondary phases after sintering at 1250 °C in air.

Lattice parameters *a* and *c* of the heat-treated apatite samples were nearly similar to the standard HA (ICDD:9-432), indicating its hexagonal crystal structure. A slight decrease of cell parameters were evidenced in heat-treated (900 °C) samples due to the ionic substitution in the HA lattice. In particular, the heat-treated NHA showed a decrease in *a* value from 9.448 to 9.447 Å in NApF2 due to multiple ionic substitutions, similar to the decrease of *c* value from 6.895 to 6.886 Å. In general, lattice parameter changes in carbonated HA are due to CO_3^{2-} substitution at PO_4^{3-} sites with reduction in parameter a and an increase in c parameter because of ionic difference [31]. However, such trend was not observed in the present study even though significant amount of CO_3^{2-} content was detected in the heat-treated NHA (2.09 wt%), NApF1 (2.49 wt%) and NApF2 (2.69 wt%) at 900 °C in CO_2 atmosphere. Since some ions, Mg^{2+}=0.65 Å and Na^{+}=0.98 Å [17,32], have smaller ionic radius compared to K^{+}=1.33 Å and Ca^{2+}=0.99 Å [3,32], it was predicted that the decrease in lattice parameters are owing to the influence of Mg content, which has the highest portion in the as-prepared powders. Both alkali ions and CO_3^{2-} have compensated the changes in lattice parameters to the extent that a decrease in both *a* and *c* parameters were observed. Sintering of NApF2 at 1250 °C in ambient condition showed opposite changes in lattice parameters with respect to sintered NHA whereby both a and c parameters increased from 9.416 to 9.432 Å and 6.880 to 6.889 Å, respectively, in the absence of CO_3^{2-}. This is also predicted to be influenced by other ion dopants in the HA structure. The heat treatment of the samples in CO_2 controlled atmosphere with less inert condition revealed almost similar CO_3^{2-} content even though the initial amount in the as-prepared samples were higher in NApF1 (3.45 wt%) and NApF2 (4.94 wt%) with almost 28 and 46% CO_3^{2-} loss, respectively. However, exceptionally, in as-prepared NHA the initial amount of CO_3^{2-} (1.69 wt%) was lower than the heat treated sample with almost 24% CO_3^{2-} gain after heat treatment. Therefore, it was difficult to predict whether the CO_3^{2-} loss was due to the surface adsorption or the structural carbonate groups as presence of air is not negligible and could contribute to the loss of substituted carbonate [33]. In the heat-treated NHA, the carbonate amount is higher than in the as-prepared samples indicating the additional carbonate substitution from CO_2 flux at 900 °C. The sintering of all the samples in air at 1250 °C yield massive carbonate loss to less than 0.2 wt%, confirming the structural carbonate loss in the samples. The heat-treatment in air at 900 °C has largely reduced the carbonate content in both stoichiometric and ions doped nanoapatite with almost 1.2 wt% retained in the samples

due to the structural carbonate loss. This indicates that the presence of CO_2 flux is highly necessary to prevent carbonate loss from the nanoapatite structure during the heat treatment.

Fig. 10 shows the FTIR spectra of the heat treated samples corresponding to HA characteristic bands for both stoichiometric and ionic doped nanoapatites. The FTIR analysis pointed out that a mixture of B type carbonation (bending and stretching bands at 875 and 1410 cm^{-1}, respectively), A+B type carbonation (bending signals at 1457 cm^{-1}) and A-type carbonation (bending band around 1548 cm^{-1}) have occurred during the heat-treatment [6,29]. The absorption intensities for the structural CO_3^{2-} in the heat treated samples are more pronounced with increasing initial CO_3^{2-} content of the as-prepared samples; in increasing order of NHA, NApF1 and NApF2. Since the heat treatment was carried out in a controlled atmospheric furnace rather than in an inert condition, high CO_3^{2-} loss was observed in the heat-treated samples. A well resolved HA characteristic bands for PO_4^{3-} at 1086, 1021, 960, 597 and 560 cm^{-1} were observed in all heat-treated powders due to its high crystallinity after the heat treatment. Bands near 3570 and 630 cm^{-1} are assigned to stretching and vibrational modes, respectively, of the hydroxyl group OH^-, which are the characteristic bands corresponding to HA. The absence of CO_3^{2-} characteristic IR bands in sintered powder samples (Fig. 11) were explained by the samples' decomposition at 1250 °C in air, resulting in pure HA phase without secondary phases despite multiple alkali ions substituted in NApF2 which is also supported by XRD patterns (Fig. 9). Moreover, both spectra showed no significant difference in the characteristic bands corresponding to HA. Well resolved HA characteristic bands for PO_4^{3-} at 1086, 1021, 960, 597 and 560 cm^{-1} were observed in sintered powders due to high crystallinity of the powder samples after heat treatment. Bands near 3570 and 630 cm^{-1} are assigned to stretching and vibrational modes, respectively, of the hydroxyl group, OH^-, which are the characteristic bands corresponding to HA. Both formulations yield carbonate free powders upon firing at

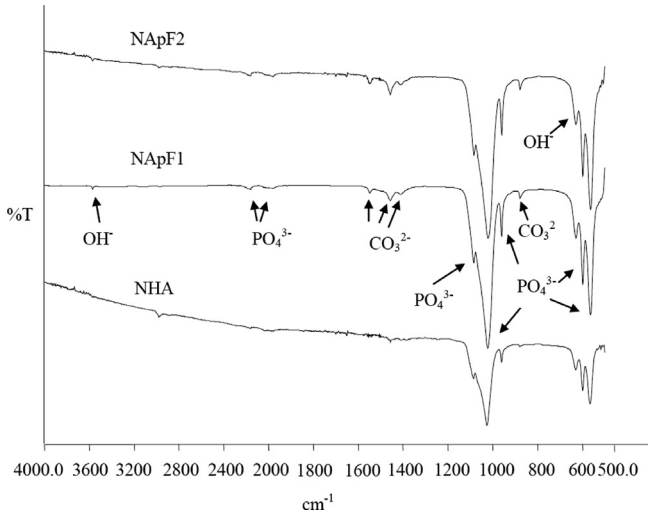

Fig. 10. FTIR spectra of stoichiometric HA (NHA) and ionic doped apatite (NApF1 and NApF2) powders synthesised at 37 & 85 ± 2 °C (reaction method II) using 1.5 M equimolar precursors after heat-treatment at 900 °C in CO_2 controlled atmosphere.

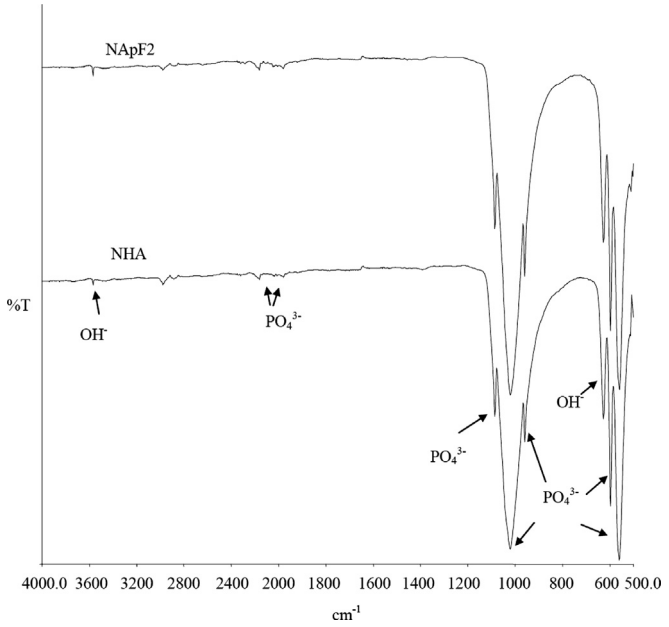

Fig. 11. FTIR spectra of stoichiometric HA (NHA) and ionic doped apatite (NApF2) powders synthesised at 37 & 85 ± 2 °C (reaction method II) using 1.5 M equimolar precursors after sintering at 1250 °C in air.

1250 °C in air without phase decomposition that confirmed the thermal stability of these powders at high temperatures.

3.3. Cytotoxicity assessment

In order to assess the biocompatibility of a material, it is important to perform an initial screening on the material's toxicity effect towards tested biological cells. Thus, the level of toxic leacheables of NHA and NApF2 samples were quantitatively evaluated on human skin fibroblast cells. The quantitative cytotoxic test results are presented in Fig. 12. It shows the cell viability for fibroblast proliferation in the presence of 100% extracts obtained from NHA and NApF2 samples. There was no significant difference in the percentage of viable cells between all the test samples in 100% extracts, indicating that the test samples have equally viable cells despite presence of alkali dopants. These results showed good cell viability on all nanoapatite powders, indicating that alkali dopants content had no deleterious effect on fibroblast proliferation.

4. Conclusion

In conclusion, a simple synthesis route has been developed to prepare multiple ions doped nanoapatite powders at high temperature without the usage of alkali agents to control the pH of precipitate, which contains essential ions found in natural bone mineral. The significance of this approach is that the apatite precipitation at high temperature with "self-controlled" pH (6–12) without the utilisation of alkali agents makes the whole synthesis easier and more suitable for industrialisation. Moreover, the cystallinity of the doped powders were increased due to the high temperature route employed in this study. Therefore, this study clearly evidenced

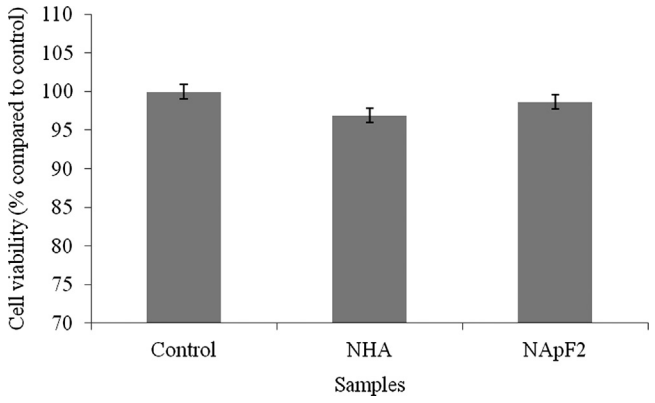

Fig. 12. The effect of 100% sample extracts on fibroblast proliferation assessed for 24 h using MTT Assay.

that increasing the synthesis temperature and varying reactant concentration yield larger apatite nuclei with higher crystallinity compared to low temperature synthesis. Despite the increase, those particles remained nanosized. Another significance is that the amount of Mg ion substitution in the apatite structure is 3 folds higher than in literature reports that using similar synthesis routes. As expected, an effective increase in carbonate composition (4.94 wt%) was observed with increasing carbonate source addition during synthesis, which is parallel to the biological hydroxyapatite (4–8 wt%). Even though the Na and K contents are not up to the composition of the biological apatite, the presence of these ions at lower concentration is expected to play a role in the biochemistry of hard tissue as the ion substitutions in the apatite phase may vary depending on the individual. The heat treatment of stoichiometric HA and multiple ions doped nanoapatite showed presence of HA phase without secondary phases, indicating its thermal stability. In addition, the cytotoxic testing suggested that the growth of fibroblast cells in the presence of both apatite extracts remained largely unaffected, indicating that the nanoapatite powders prepared using this technique have no cytotoxic potential to HSF 1184.

Acknowledgements

The authors acknowledge the support of SIRIM Berhad, Malaysian Ministry of Higher Education and Universiti Teknologi Malaysia (Tier-1 vote J130000.7136.00H54) for sponsoring the project. The authors also thank Miss Zulaika Miswan for her constructive comments on the language.

References

[1] S.V. Dorozhkin, Nanosized and nanocrystalline calcium orthophosphates, Acta Biomaterialia 6 (2010) 715–734.
[2] D. Laurencin, N. Almora-Barrios, N.H. de Leeuw, C. Gervais, C. Bonhomme, F. Mauri, W. Chrzanowski, J.C. Knowles, R.J. Newport, A. Wong, Z. Gan, M.E. Smith, Magnesium incorporation into hydroxyapatite, Biomaterials 32 (2011) 1826–1837.
[3] S. Kannan, J.M.G. Ventura, J.M.F. Ferreira, Synthesis and thermal stability of potassium substituted hydroxyapatites and hydroxyapatite/β-tricalciumphosphate mixtures, Ceramics International 33 (2007) 1489–1494.
[4] C. Kothapalli, M. Wei, A. Vasiliev, M.T. Shaw, Influence of temperature and concentration on the sintering behaviour and mechanical properties of hydroxyapatite, Acta Materialia 52 (2004) 5655–5663.
[5] M. Pretto, A.L. Costa, E. Landi, A. Tampieri, C. Galassi, Dispersing behaviour of hydroxyapatite powders produced by wet-chemical synthesis, Journal of American Ceramic Society 86 (2003) 1534–1539.
[6] E. Landi, A. Tampieri, M. Mattioli-Belmonte, G. Celotti, M. Sandri, A. Gigante, P. Fava, G. Biagini, Biomimetic Mg- and Mg, CO_3-substituted hydroxyapatites: synthesis characterization and in vitro behaviour, Journal of the European Ceramic Society 26 (2006) 2593–2601.
[7] S. Kannan, S.I. Vieira, S.M. Olhero, P.M.C. Torres, S. Pina, O.A.B. da Cruz e Silva, J.M.F. Ferreira, Synthesis, mechanical and biological characterization of ionic doped carbonated hydroxyapatite/β-tricalcium phosphate mixtures, Acta Biomaterialia 7 (2011) 1835–1843.
[8] S.R. Kim, J.H. Lee, Y.T. Kim, D.H. Riu, S.J. Jung, Y.J. Lee, S.C. Chung, Y.H. Kim, Synthesis of Si, Mg substituted hydroxyapatites and their sintering behaviors, Biomaterials 24 (2003) 1389–1398.
[9] S. Sprio, A. Tampieri, E. Landi, M. Sandri, S. Martorana, G. Celotti, G. Logroscino, Physico-chemical properties and solubility behaviour of multi-substituted hydroxyapatite powders containing silicon, Materials Science and Engineering C 28 (2008) 179–187.
[10] E. Landi, A. Tampieri, G. Celotti, S. Sprio, M. Sandri, G. Logroscino, Sr-substituted hydroxyapatites for osteoporotic bone replacement, Acta Biomaterialia 3 (2007) 961–969.
[11] S. Ramesh, C.Y. Tan, R. Tolouei, M. Amiriyan, J. Purbolaksono, I. Sopyan, W.D. Teng, Sintering behaviour of hydroxyapatite prepared from different routes, Materials & Design 34 (2012) 148–154.
[12] I. Sopyan, S. Ramesh, M. Hamdi, Synthesis of nano sized hydroxyapatite powder using sol–gel technique and its conversion to dense and porous bodies, Indian Journal of Chemistry 47 (2008) 1626–1631.
[13] E. Landi, A. Tampieri, G. Celotti, S. Sprio, Densification behaviour and mechanisms of synthetic hydroxyapatites, Journal of the European Ceramic Society 20 (2000) 2377–2387.
[14] V. Uskoković, D.P. Uskoković, Nanosized hydroxyapatite and other calcium phosphates: chemistry of formation and application as drug and gene delivery agents, Journal of Biomedical Materials Research Part B: Applied Biomaterials 96B (2011) 152–191.
[15] T.A. Kuriakose, S.N. Kalkura, M. Palanichamy, D. Arivuoli, K. Dierks, G. Bocelli, C. Betzel, Synthesis of stoichiometric nano crystalline hydroxyapatite by ethanol-based sol–gel technique at low temperature, Journal of Crystal Growth 263 (2004) 517–523.
[16] Y.X. Pang, X. Bao, Influence of temperature, ripening time and calcination on the morphology and crystallinity of hydroxyapatite nanoparticles, Journal of the European Ceramic Society 23 (2003) 1697–1704.
[17] I. Cacciotti, A. Bianco, M. Lombardi, L. Montanaro, Mg-substituted hydroxyapatite nanopowders: synthesis, thermal stability and sintering behaviour, Journal of the European Ceramic Society 29 (2009) 2969–2978.
[18] E. Boanini, M. Gazzano, A. Bigi, Ionic substitutions in calcium phosphates synthesised at low temperature, Acta Biomaterialia 6 (2010) 1882–1894.
[19] S. Lazic, S. Zec, N. Miljevic, S. Milonjic, The effect of temperature on the properties of hydroxyapatite precipitated from calcium hydroxide and phosphoric acid, Thermochimica Acta 374 (2001) 13–22.
[20] Z.Y. Li, W.M. Lam, C. Yang, B. Xu, G.X. Ni, S.A. Abbah, K.M.C. Cheung, K.D.K. Luk, W.W. Lu, Chemical composition, crystal size and lattice structural changes after incorporation of strontium into biomimetic apatite, Biomaterials 28 (2007) 1452–1460.
[21] R.N. Panda, M.F. Hsieh, R.J. Chung, T.S. Chin, FTIR, XRD, SEM and solid state NMR investigations of synthesised by hydroxide-gel technique, Journal of Physics and Chemistry of Solids 64 (2003) 193–199.
[22] I. Bogdanoviciene, A. Beganskiene, K. Tõnsuaadu, J. Glaser, H.J. Meyer, A. Kareiva, Calcium hydroxyapatite, $Ca_{10}(PO_4)_6(OH)_2$ ceramics prepared by aqueous sol–gel processing, Materials Research Bulletin 41 (2006) 1754–1762.
[23] A. Costescu, I. Pasuk, F. Ungureanu, A. Dinischiotu, F. Huneau, S. Galaup, P.L.E. Coustumer, D. Predoi, C. Ftir, Physico-chemical

properties of nano-sized hexagonal hydroxyapatite powder synthesised by sol–gel, Journal of Nanomaterials 5 (2010) 989–1000.
[24] E. Landi, A. Tampieri, G. Celotti, L. Vichi, M. Sandri, Influence of synthesis and sintering parameters on the characteristics of carbonate apatite, Biomaterials 25 (2004) 1763–1770.
[25] N. Rameshbabu, T.S. Sampath Kumar, T.G. Prabhakar, V.S. Sastry, K.V.G.K. Murty, K. Prasad Rao, Antibacterial nanosized silver substituted hydroxyapatite: synthesis and characterization, Journal of Biomedical Materials Research Part A 80A (2007) 581–591.
[26] Y.E. Greish, J.L. Sturgeon, A. Singh, N.R. Krogman, A.H. Touny, S. Sethuraman, L.S. Nair, C.T. Laurencin, H.R. Allcock, P.W. Brown, Formation and properties of composites comprised of calcium-deficient hydroxyapatites and ethyl alanate polyphosphazenes, Journal of Materials Science: Materials in Medicine 19 (2008) 3153–3160.
[28] J. Gustavsson, M.P. Ginebra, E. Engel, J. Planell, Ion reactivity of calcium-deficient hydroxyapatite in standard cell culture media, Acta Biomaterialia 7 (2011) 4242–4252.
[29] S. Koutsopoulos, Synthesis and characterization of hydroxyapatite crystals: a review study on the analytical methods, Journal of Biomedical Materials Research Part A 62 (2002) 600–612.
[30] I.R. Gibson, S. Ke, S.M. Best, W. Bonfield, Effect of powder characteristics on the sinterability of hydroxyapatite powders, Journal of Materials Science: Materials in Medicine 12 (2001) 163–171.
[31] Y. Suetsugu, Y. Takahashi, F.P. Okamura, J. Tanaka, Structure analysis of A-type carbonate apatite by a single-crystal X-ray diffraction method, Journal of Solid State Chemistry 155 (2000) 292–297.
[32] H. El Feki, J.M. Savariault, A. Ben Salah, Structure refinements by the Rietveld method of partially substituted hydroxyapatite: $Ca_9Na_{0.5}(PO_4)_{4.5}(CO_3)_{1.5}(OH)_2$, Journal of Alloys and Compounds 287 (1999) 114–120.
[33] I.R. Gibson, W. Bonfield, Novel synthesis and characterization of an AB-type carbonate-substituted hydroxyapatite, Journal of Biomedical Materials Research 59 (2002) 697–708.